

Mechanical behaviour of Australian Strathbogie granite under in-situ stress and temperature conditions: An application to geothermal energy extraction



W.G.P. Kumari^a, P.G. Ranjith^{a,*}, M.S.A. Perera^b, S. Shao^a, B.K. Chen^c, A. Lashin^d, N.Al Arifi^e, T.D. Rathnaweera^a

^a Department of Civil Engineering, Monash University, Building 60, Melbourne, Victoria 3800, Australia

^b Department of Infrastructure Engineering, Building block D, The university of Melbourne, Parkville, Melbourne, 3010, Australia

^c Department of Mechanical & Aerospace Engineering, Monash University, Building 36, Melbourne, Victoria 3800, Australia

^d King Saud University, College of Engineering, Petroleum and Natural Gas Engineering Department, P.O. Box 800, Riyadh 11421, Saudi Arabia

^e King Saud University, College of Science, Geology and Geophysics Department, P.O. Box 2455, Riyadh 11451, Saudi Arabia

ARTICLE INFO

Article history:

Received 18 May 2016

Received in revised form 20 July 2016

Accepted 25 July 2016

Keywords:

Geothermal energy
Granite
High temperature
Stress-strain response
Triaxial
Acoustic
XRD

ABSTRACT

Geothermal heat has now been identified as an effective renewable energy source due to severe environmental impacts created by conventional fossil usage on global climatic change. However, its wide application has been limited due to the lack of knowledge, particularly of the geothermal conditions of reservoir rocks at elevated temperatures and pressures. Such high temperatures and pressures possibly alter the mechanical properties of reservoir rocks due to the associated micro-structural and mineralogical alterations of the rock mass, which are an important attribute for wellbore stability and stimulation of geothermal reservoirs for safe and effective geothermal energy extraction. This study therefore investigates the stress-strain behaviour under in-situ stress and temperature conditions by conducting a series of high-pressure, high-temperature tri-axial experiments on Australian Strathbogie granite under four different confining pressures (10, 30, 60, 90 MPa) and four different temperatures (RT, 100, 200, 300 °C). The effect of temperature on the mechanical behaviour of rock specimens was studied under tri-axial conditions and the corresponding fracture propagation behaviour was observed using an advanced acoustic emission (AE) system. The corresponding micro-structure alteration in granite was observed using SEM analysis. According to the findings, increasing temperature leads to an initial increment in reservoir rock strength and shear parameters followed by reduction, and the trend is aligned with the crack formation pattern of the rock mass. This was further confirmed by the SEM analysis, according to which the rock micro-structure is subject to only minor changes at relatively low temperatures and higher temperatures cause micro-cracks to develop along the rock mass grain boundaries. Furthermore, the conventional Mohr-Coulomb criteria failed to model the stress-strain response of rock under geothermal reservoir conditions, and was therefore modified for the corresponding in-situ conditions.

© 2016 Elsevier Ltd. All rights reserved.

1. Introduction

Geothermal heat has been identified as a renewable and reliable energy source, given the severe environmental impacts created by conventional fossil fuels such as coal and oil (Martín-Gamboa et al., 2015; Axelsson, 2010). Exploratory geothermal wells have therefore been drilled to test the availability of geothermal reservoir

* Corresponding author at: Deep Earth Energy Laboratory, Department of Civil Engineering, Monash University, Building 60, Melbourne, Victoria 3800, Australia.

E-mail address: ranjith.pg@monash.edu (P.G. Ranjith).

rocks (rocks at elevated temperatures) and deep granite reservoirs have been found to have adequate temperatures to serve as a geothermal reservoirs (Fox et al., 2013). Such explorations involve finding vast blocks of “hot rocks” with fracture systems. Such rocks can be used to generate electricity. In this process, water is first injected and circulated through the fractures in the geothermal reservoirs and eventually pumped back to the surface as steam. However, the exploration of geothermal resources has become a challenge to engineers and geologists, due to the high temperature and stress environments in geothermal reservoirs. For this reason, laboratory experiments conducted under high pressure and temperature conditions (geothermal conditions) can assist in providing

basic predictions. A large number of laboratory experiments has therefore been conducted since 1970 to investigate the influence of high pressure and temperature on rock in relation to geothermal heat extraction (Saratovich et al., 2016), deep geological disposal of nuclear waste (Paquet and François, 1980), deep mining (Wawersik and Hannum, 1980) and geological CO₂ storage (Dai et al., 2014).

The mechanical behaviour of reservoir rocks is significantly influenced by elevated temperatures, because they cause the micro-structure of the rock mass to be altered through thermal expansion, the development of new micro-cracks, extending and/or widening the existing micro-cracks and various mineralogical alterations. Rock strength-deformation criteria change with temperature, and some rock mechanical properties, such as compressive strength, tensile strength, elastic modulus, cohesive strength and friction angle, decrease with increasing temperature (Heuze, 1983; Dwivedi et al., 2008). However, such alterations are also affected by the confinement applying on the rock mass, and confining pressure causes the suppression of thermal cracks and the extension/widening of existing micro-cracks. This results in further alteration of the rock mass mechanical properties, resulting in changing failure modes (Mogi, 1966). Studies have identified the transition of rock failure mode from brittle to ductile with increasing confinement. However, this transition is diverse due to the different mineralogical compositions and grain boundaries in different rocks (Klein et al., 2001; Wong, 1982).

Although many studies have been conducted to investigate the temperature-dependent mechanical behaviour of reservoir rocks, most experiments have been conducted in unconfined environments (Singh et al., 2015; Shao et al., 2014). Pre-heating the specimens to the corresponding temperature ranges and testing at room temperatures has been frequently done (Bauer and Johnson, 1979; Xu et al., 2008), but the method is not reliable, as geothermal reservoirs experience continuous thermal stresses. Such limitations have occurred mainly due to the limited number of appropriate test facilities available to simulate the stress and temperature conditions of actual geothermal reservoirs. Although some studies have analytically and numerically evaluated the mechanical properties of rocks under high temperatures and pressures (Chester and Higgs, 1992; Tian et al., 2013; Vásárhelyi et al., 2016), to date none has captured the stress-strain behaviour and failure criteria of rocks over a wide range of confining pressures and temperatures, particularly for Australian granite. However, the thermo-elastic response and appropriate failure criteria are essential inputs for many engineering applications under high pressures and temperatures, including geothermal extraction applications. This study therefore intends to fill this gap, and it is hoped it will make an important contribution to many deep underground applications.

2. Methodology

2.1. Tested material

Granite is an abundant crystalline rock in the earth with medium to coarse grains which was formed as a result of the slow cooling of magma. Granite therefore has abundant radioactive elements (K, Th, and U). Such elements bring elevated geothermal gradients to deep granite reservoirs, which therefore have ideal conditions as geothermal reservoirs. The mineralogical composition of granite mainly consists of quartz, feldspar, plagioclase and biotite, and small amounts of muscovite, amphibole, hornblende and opaque (Dwivedi et al., 2008).

For the present study, samples were collected from the Strathbogie batholith, which is a composite granitoid intrusion body spreading over more than 1500 km² in 150 km north-east from Melbourne (Fig. 1). Strathbogie granite is a high-level, discordant

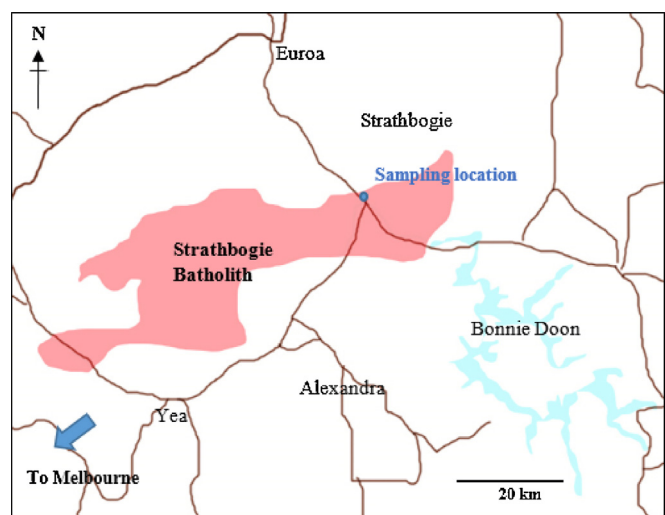


Fig. 1. Sampling location of Strathbogie batholith in central Victoria.

Table 1

Physical, mechanical and petrographic properties of Strathbogie granite (obtained under room temperature and atmospheric pressure conditions).

Rock type	Granite
Colour	White with dark brown
Average grain size	70–600 µm
Petrographic description	Mainly consists of feldspar, biotite, quartz and plagioclase Equigranular, coarse grained, S-type granite
Bulk density (kg/m ³)	2703.4
Compressive strength (MPa)	118.17
Elastic modulus (GPa)	9.09
Porosity (%)	1.16

Table 2

Results of XRD analysis.

Mineral ID	MASS%
Alpha quartz	50
Sodic and intermediate plagioclase	16
Biotite–phlogopite	15
K-feldspar	13
Clinochlore	2
Muscovite–sericite	2
Dolomite–ankerite	1
Other minerals	1

granite that mainly consists of quartz, K-feldspar, cordierite and biotite (Phillips et al., 1981). The selected granite type is coarse-grained and white and dark brown in colour with around 1.16% porosity. Fig. 2 presents a close-up view of a typical Strathbogie granite sample, an optical microscopic image and an SEM image of its thin section. As can be seen in Fig. 2(b), clear mineralogical assembling can be observed in the granite specimen, mainly with quartz, K-feldspar and plagioclase. As shown in Fig. 3, the grain size was measured from a thin section of this granite and found to be mainly in the range of 0 mm–200 µm with only a small number of larger grains (>300 mm) (Shao et al., 2014). Table 1 summarizes the physical, mechanical and petrographic properties of the tested Strathbogie granite. In addition, an XRD analysis was conducted to determine the mineralogical composition of the selected granite and the result is shown in Table 2. As the table shows, quartz is the predominant mineral in the selected granite (50%), followed by 16% of sodic and intermediate biotite and 15% of plagioclase. The mineralogical composition of this particular granitic composition is representative of the composition of the majority of the Earth's granites (Best, 1995). All the physical properties in Tables 1 and 2

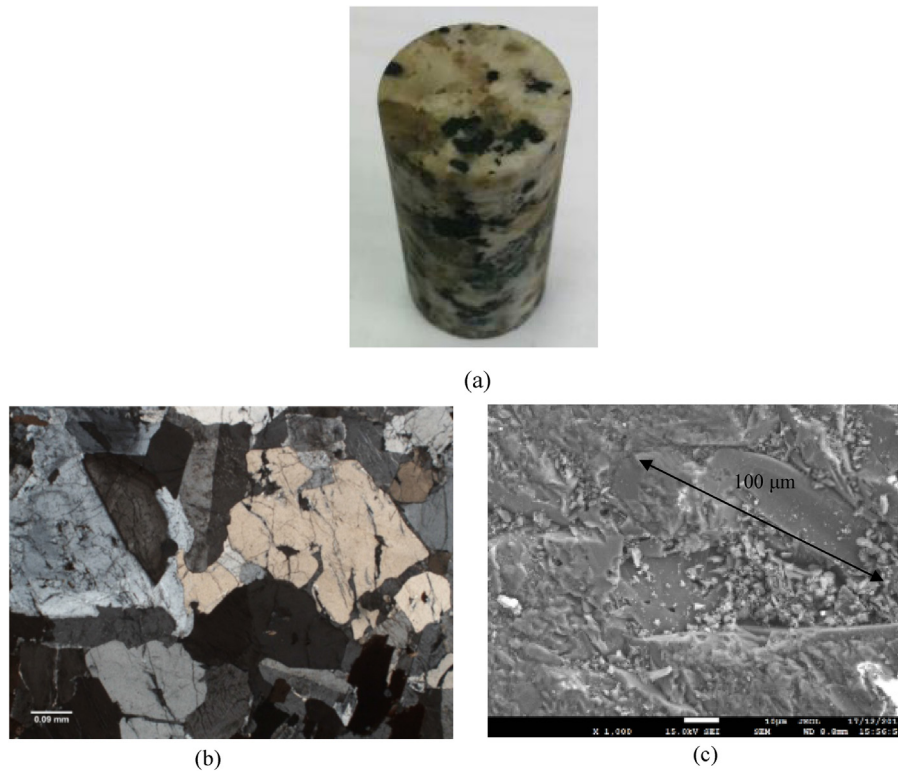


Fig. 2. (a) Close-up view of a sample (b) Microscopic image of a thin section of a sample (c) SEM image of a thin section of a sample.

were obtained by conducting various tests in the laboratory: XRD analysis (mineral composition), uniaxial compression testing (compressive strength, elastic modulus), thin section analysis (average grain size), mercury intrusion testing (porosity) and volume and weight measurement (bulk density).

2.2. Sample preparation

Sample preparation and testing were carried out at the Deep Earth Energy Research Laboratory (DEERL) in the Civil Engineering Department of Monash University, and the sample preparation was conducted in accordance with the ASTM standard for tri-axial compressive testing (ASTM D7012-10 (2010)). In order to maintain consistency, all the samples were cored to 22.5 mm in diameter using the same block of granite at the same orientation. During the sampling great care was taken to obtain samples with the same crystalline orientation, and samples with different crystalline orientation, internal layers and visible cracks were discarded. It should be noted that coring-induced rock-microstructure alteration is an important aspect to consider in laboratory experiments, although few studies have considered this effect. To avoid such issues, a very small coring rate was adopted and water was used as a lubricant. The cored specimens were then cut into 45 mm high cylinders and both ends of the specimens were ground to produce two parallel surfaces perpendicular to the axes of the cylindrical specimens.

2.3. Experimental procedure

Tri-axial experiments were conducted on samples under four different confining pressures (10, 30, 60 and 90 MPa) and four different temperatures (RT, 100, 200, 300 °C). These experimental conditions were selected, because the most preferable hot dry rock systems are generally located at depths of 2.5–3.5 km and have around 70 MPa–120 MPa confining pressures (assuming the reservoir rock density is equal to 2500 kg/m³) and temperatures of

200–350 °C (Breed et al., 2013). The different confining pressures and temperatures were selected to simulate the reservoir depth effect and to obtain a sufficient data set to understand the failure criteria under different temperatures.

The complete arrangement of the tri-axial cell is shown in Fig. 3. The prepared sample was first placed inside the cell and the required confining pressure was then applied using a silicon oil system, and an annealed copper sleeve was used to isolate the sample from the confining liquid (refer to Fig. 3(b)). A mica-insulated metal band heater was used to heat the pressure cell and consequently the rock sample. The temperatures of the cell were adjusted using a controller and a constant small heating rate of 2.5 °C/min was used to prevent micro-structural damage due to sudden thermal shocks. Two separate thermocouples were used to achieve precise temperature control, and the reading of the thermocouple installed inside the cell (Fig. 3(b)) was recorded by the data acquisition system. The other thermocouple that was attached to the barrel (Fig. 3(a)) was used to control the band heater. Furthermore, the barrel and the top of the pressure cell were covered using an insulating blanket to reduce heat loss during the experiments and to minimise the influence of air flows towards the cell. All the tests were started once the system had achieved a steady state to ensure uniformity in temperature and pressure across the sample. Equilibrium was ensured by monitoring the confinement pump volume and the thermocouple readings inside the cell (located very close to the specimen). Under steady-state conditions, constant pump volume and constant temperature were observed and testing was initiated. A constant loading pump flow rate of 1 ml/min was adopted for all the test specimens and the converted displacement rate was 0.05 mm/min. It should be noted that a small shaft resistance exists as a result of the sealing of the hydraulic cylinder, and this effect was considered in the calibration of the loading cell. The sealing resistance was obtained by measuring the pump pressure to initiate a movement in the loading shaft, and this was deducted from each pressure reading to eliminate the resistance of the sealing dur-

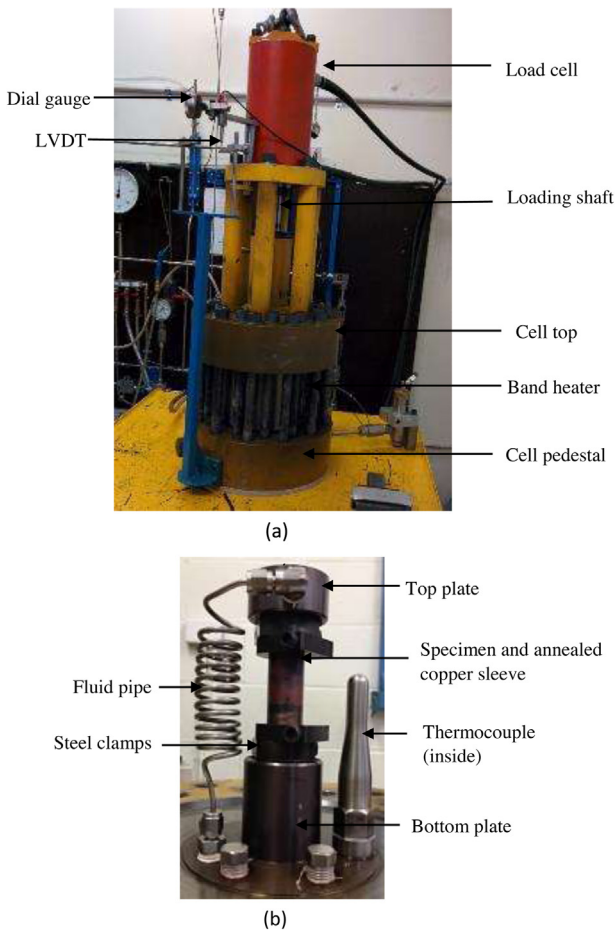


Fig. 3. (a) High-pressure, high-temperature tri-axial machine (b) Inside view of the cell.

ing calibration. However, it should be noted that, compared to the large axial load, this resistance is negligible which is only 0.19% of maximum measurement. During the load application, the axial strain was measured using linear variable differential transducers (LVDTs) attached to the ram of the load cell (Fig. 3(a)).

An acoustic emission (AE) system was also employed in the testing of samples to record the data related to the fracturing process. The AE system adopted was a peripheral component interconnection (PCI) system with a nominal resolution frequency of 500 kHz. During the experiments, two sensors were attached to either side of the loading shaft and with the external amplifiers, which generated low frequency acoustic waves with the fracturing of the sample. In addition, possible micro-structural and mineralogical changes that occurred during thermal and confinement effects were checked using SEM analyses.

3. Results and discussion

3.1. The overall stress-strain response

The influence of temperature on the stress-strain behaviour of the tested granite was considered first and the test results (deviatoric load at failure, deviatoric stress at failure, triaxial compressive strength and elastic modulus) are given in Table 3. Fig. 4 illustrates the relationships between deviatoric stress and axial strain curves for the samples tested at 10, 30, 60 and 90 MPa confining pressures at various temperatures (20, 100, 200, 300 °C). In relation to the stress-strain curves of the Strathbogie granite under tri-axial loading, the corresponding failure modes were characterized

using the typical Mohr-Coulomb brittle deformation. The deviatoric stress-strain plots of the granite samples (Fig. 4) exhibited concave upward curvilinear trends from initial loading to the peak value, beyond which strain softening occurred, causing a rapid stress drop to a residual value. Increasing peak stress with increasing confining pressure can be observed, which is to be expected, according to typical Mohr-Coulomb type brittle failure (Paterson and Wong, 2005).

Traditionally, rock failure in compression can occur in two main ways; (a) dilatancy and failure by strain softening under relatively low confining pressures and (b) failure by strain hardening under elevated confining pressures, and a transitional regime may be observed at intermediate pressures. These transitional failure modes have been referred to as “quasi-brittle”, and complex localized features such as conjugate shear bands can be observed under such conditions (Klein et al., 2001; Gajo et al., 2004). By visual inspection of the post-failure samples, important information about the alteration of the granite failure mechanism with confining pressures and temperatures can be identified. Post-failure images (Fig. 5) were therefore collected after each test.

According to the post-failure images, specimens that failed at 10–60 MPa confining pressures mainly failed by shear localization along an inclined macroscopic shear band with a single shear zone across each sample. However, samples tested at higher confinements of 90 MPa and 120 MPa (at 100 °C) exhibited strain hardening characteristics after achieving the peak stress, and several conjugate shear bands could be observed on the cylindrical sample surface, instead of the single shear band observed earlier. This characteristic was significant at 120 MPa confining pressure. However, it should be noted that only one test was conducted at 120 MPa confinement, because at such high confining pressures the corresponding failure load of granite exceeds the bottom pedestal's load-bearing capacity. Further, a progressive reduction was observed in the failure plane angle with respect to the minor principal stress direction with increasing confining pressure, which implies a reduction in friction angle, possibly due to the greater quasi-brittle behaviour that was shown by granite samples at higher confining pressures (Wong et al., 2001).

3.2. Effect of temperature and confining pressure on mechanical properties of Strathbogie granite

Fig. 6 illustrates the influence of temperature on the deviatoric stress of the tested granite under each confinement. As the figure shows, the influence of confinement is more significant than that of temperature in the temperature range considered here. Wong and Brace (1979) confirm that at lower confining pressures considerable thermal cracking occurs at relatively low temperatures. If thermal cracking is responsible for the reduction in failure strength, a sharp reduction in deviatoric stress with increasing temperature (with suppression of thermal cracks) should be exhibited under unconfined pressure condition. However, based on the experimental results, under unconfined conditions, up to 100 °C, 17.6% of increment in deviatoric stress is followed by 2.5% and 10.5% reductions at 200 °C and 300 °C, respectively. However, when confinement was applied, strength reduction was initiated after a higher temperature of 200 °C, mainly due to the inhibition of thermal cracks by induced compressive force. Thermal cracking is therefore an important strength property alteration mechanism in reservoir rocks under certain confining pressure conditions.

A clear influence of temperature on deviatoric stress at any depth or confinement can be observed, and increasing the temperature from room temperature to 200 °C causes an increment in deviatoric stress, and further increasing of temperature to 300 °C causes a slight reduction in it. This is because the thermal expansion which occurs with increasing temperature causes the reduction of

Table 3

Mechanical properties of Strathbogie granite at different test temperatures and pressures.

Temperature (°C)	Confining Pressure (MPa)	Deviatoric load at failure (kN)	$\sigma_1 - \sigma_3$ (MPa)	σ_1 (MPa)	Elastic modulus (GPa)
RT	0	47.0	118.2	118.2	9.1
	10	90.9	186.9	196.9	18.3
	30	175.4	311.9	341.9	21.6
	60	281.6	422.5	482.5	22.3
	90	371.3	503.3	593.3	22.5
100	0	55.2	139.0	1390	8.9
	10	104.6	225.5	235.5	19.3
	30	183.5	333.7	363.7	23.0
	60	271.0	440.9	500.9	23.3
	90	368.6	510.3	600.3	22.7
	120	450.3	568.9	688.9	24.2
200	0	53.9	135.53	135.5	8.5
	10	116.7	258.25	268.2	20.2
	30	195.9	374.42	404.4	23.4
	60	316.6	508.98	5690	24.1
	90	383.2	549.6	639.6	25.4
300	0	50.2	126.3	126.3	8.0
	10	93.6	249.4	259.4	20.1
	30	195.7	367.5	397.5	23.2
	60	272.1	464.6	524.6	23.8
	90	306.0	516.5	606.5	24.6

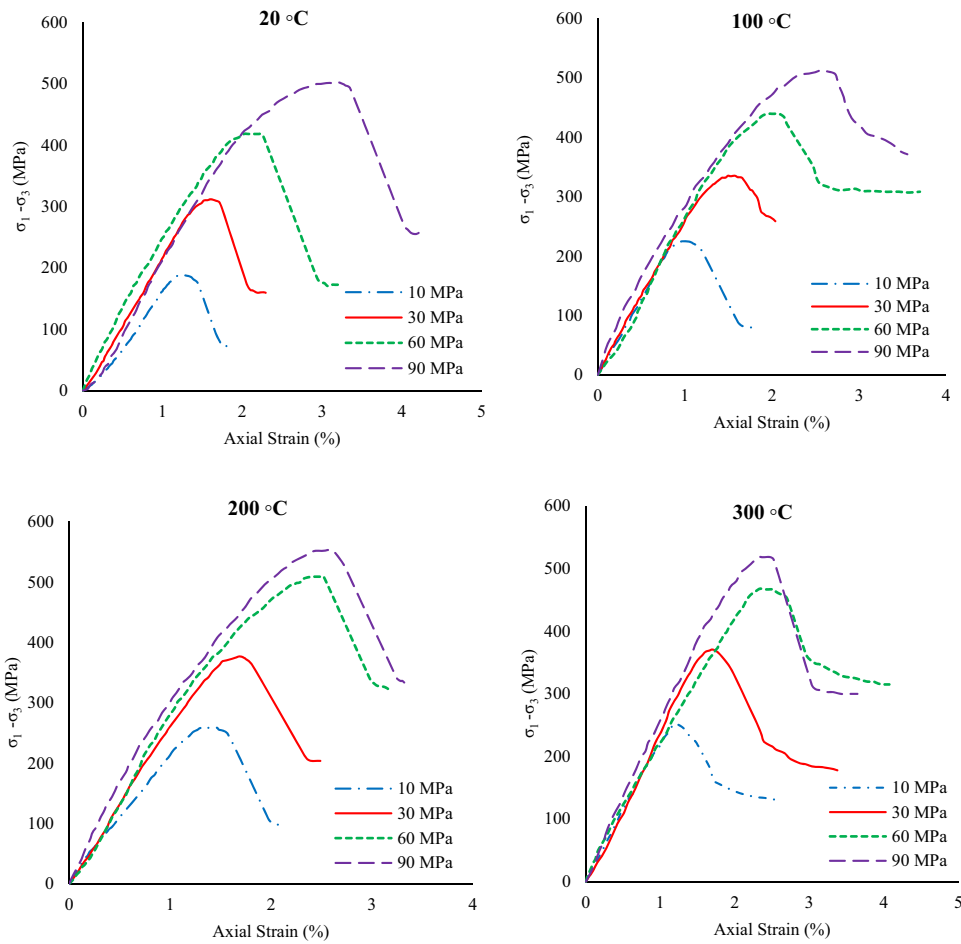
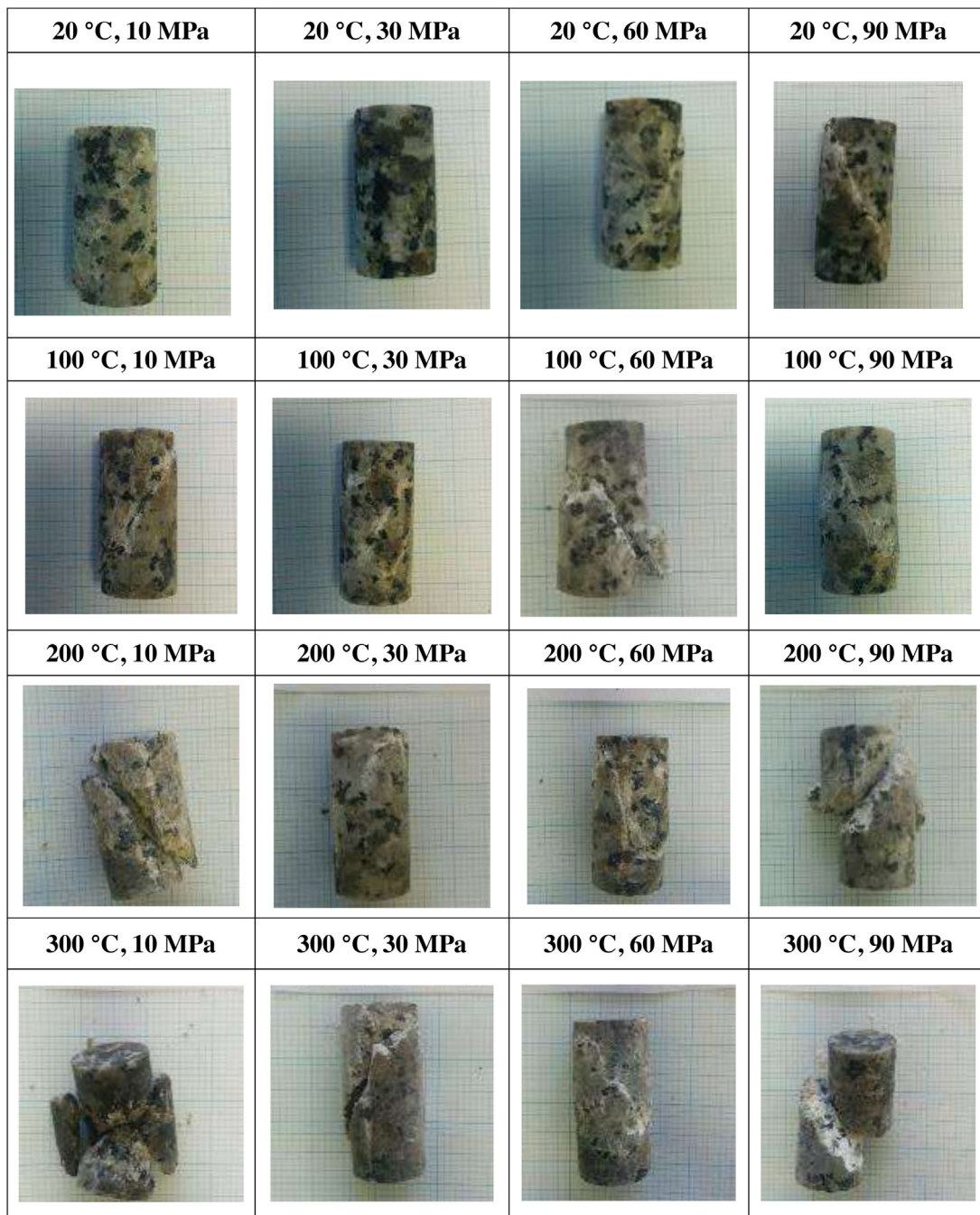


Fig. 4. Corresponding stress–strain responses of granite at different temperatures.

the distance between the interfaces of individual minerals, which increases their mutual attraction and bonding strength (Dmitriev, 1972). However, further increase of temperature causes the crystalline particles of the rock mass to fracture through pre-existing grain boundaries between mineral grains with different thermo-

elastic moduli and thermal conductivities, resulting in reduced rock strength (Kranz, 1983; Homand-Etienne and Houptet, 1989). According to the tri-axial experimental studies conducted by Wong (1982) and Tullis and Yund (1977), increasing the temperature leads to reduction in the failure stress of Westerly granite under any

**Fig. 5.** Post-failure images of tested specimens.

confining pressure. The reductions of strength characteristics were relatively small up to 500 °C and beyond that an accelerated downward trend was identified. Furthermore, wider localized zones were observed at high temperatures in the post-failure images. However, these studies were conducted at wider temperature ranges (up to 700 °C and 900 °C, respectively) and the researchers therefore did not pay close attention to reservoir rock behaviour under relatively low geothermal temperature ranges (<300 °C). This was the focus of the present study, according to which there is an initial strengthening and stiffening in granite with increasing temperature at low temperatures (up to 200 °C), and increasing the temperature beyond a certain value causes a gradual reduction in failure stress with increasing temperature. Elastic modulus is an important mechanical property of any reservoir rock, and

describes the brittle characteristics of the rock mass. It is therefore often used to evaluate many in-situ stress applications, including wellbore stability, fracturing possibility and tectonic stress distribution (Heard and Page, 1982). The temperature-dependent brittle properties (elastic modulus) of the tested granite were then evaluated. The elastic region of each stress-strain curve was used to calculate the temperature- and pressure-dependent Young's moduli (E) and the results are shown in Fig. 7. The axial strain was measured using LVDTs attached to the loading ram with a linearity error of $\pm 0.1\%$ F.S (full scale) (± 0.0075 mm) and infinite resolution (no hysteresis). An increment of the modulus of Strathbogie granite with increasing temperature up to 200 °C can be observed, and further increase of temperature (to 300 °C) causes the elastic modulus to be slightly reduced for any confinement. This trend is

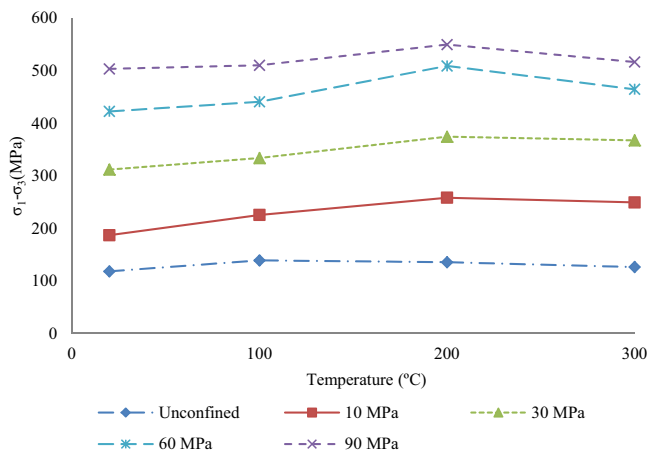


Fig. 6. Variation of deviatoric stress with different temperatures under tested confining pressures.

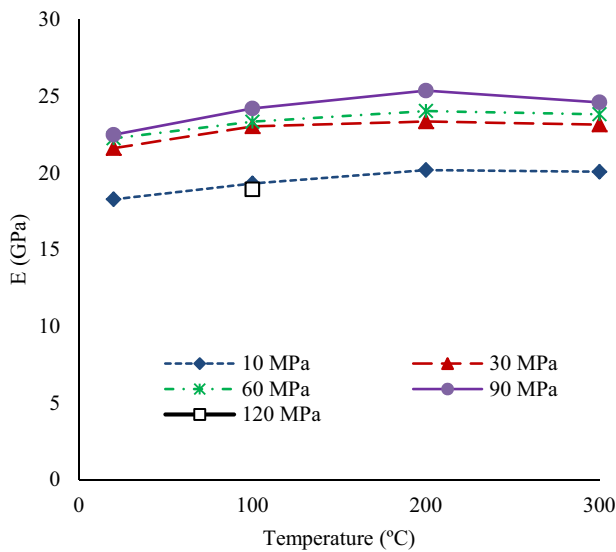


Fig. 7. Variation of elastic modulus versus confining pressure for different temperatures.

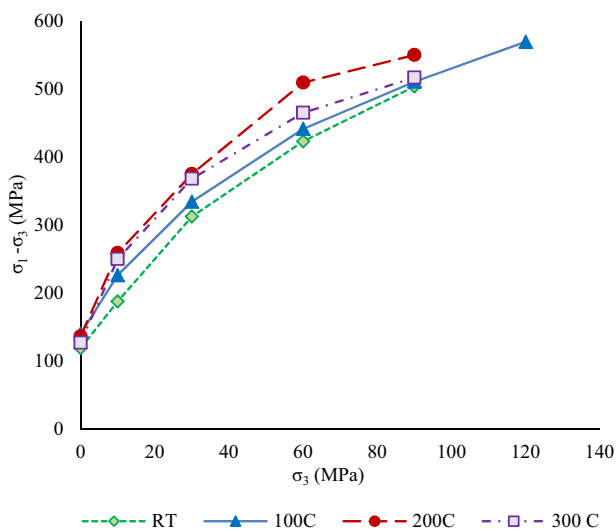


Fig. 8. Variation of deviatoric stress versus confining pressure for different temperatures.

consistent with the temperature-dependent strength behaviour of the granite described above. The reason for the initial elastic module increment may be that the specimen becomes more brittle at the initial temperature ranges due to thermally-induced volumetric expansion and the associated pore volume reduction. The later slight reduction of Young's modulus with increasing temperature exhibits an enhancement in ductile behaviour (quasi-brittle characteristics) with further increase of temperature. This is possibly due to the increased crack density caused by the induced thermal crack development and the related weakening of the granite.

A general increment in elastic modulus with increasing confinement can be observed until 90 MPa, and a further increase of confinement (to 120 MPa) reduces the Young's modulus considerably. With increasing confining stress additional plastic deformation occurs, exhibiting strain-hardening characteristics in granite under high confinements. However, within the range of the experiments conducted (10 MPa–120 MPa) it cannot be definitively identified as a 'brittle' or 'ductile' regime. However, the strain-hardening behaviour observed at 120 MPa indicates transitional characteristics and this can be identified as 'quasi-brittle' behaviour (Klein et al., 2001). The initial Young's modulus reduction with increasing confinement was observed by Heard and Page (1982), who conducted tests up to 55 MPa confining pressure. However, the latter behaviour was not observed by these researchers. Interestingly, according to the research literature, at low temperatures (<200 °C) some granite types are more temperature-sensitive, while in contrast, some granites are more temperature-sensitive at high temperatures. The initial strength enhancement is more significant for coarse-grained granites and granodiorite than for fine-grained granites. For example, according to Heard and Page (1982), Stripa granite is more sensitive to temperature at relatively low temperatures (<200 °C), and Westerly granite is more sensitive to temperature at high temperatures (>200 °C). Such contradictory behaviours may occur in granite due to the different grain size distributions, grain orientations, mineralogical compositions and heterogeneity of different granite types. This indicates the importance of studying the mineralogical composition and microstructural influence of granites on such on temperature-dependent strength variations.

3.3. Effect of temperature on shear strength parameters of Strathbogie granite

Fig. 8 illustrates the variation of deviatoric stress of the tested granite with confining pressure for each temperature. The figure shows that increasing confinement causes the granite's deviatoric stress to increase non-linearly and gradually come to a steady state. This is consistent with similar previous studies, which have clearly shown the enhancement of rock strength with increasing confinement, and the increasing rate is reduced with increasing confining pressure (Barton, 2013; Singh et al., 2011). This is because at low confining pressures there is a high dilation potential. Therefore, the ability to open rock micro-cracks is high, resulting in higher friction angles. However, this dilation potential and the corresponding tendency for micro-cracks to open are suppressed with increasing confinement, resulting in lower friction angles at higher confining pressures. Therefore, the failure mechanism of the rocks shifts from brittle to ductile with increasing confinement, changing the shape of the Mohr-Coulomb failure envelope, and according to Barton (1976), at critical confining pressure the Mohr-Coulomb failure envelope reaches a zero gradient. This has also been shown by Hoek (1983). The present study has clearly identified this rock behaviour in the Mohr-Coulomb failure envelopes developed for each temperature condition (refer to Fig. 9). According to Fig. 9, the traditional linear Mohr-Coulomb criteria are applicable only in the brittle region of the failure envelope, and at higher confine-

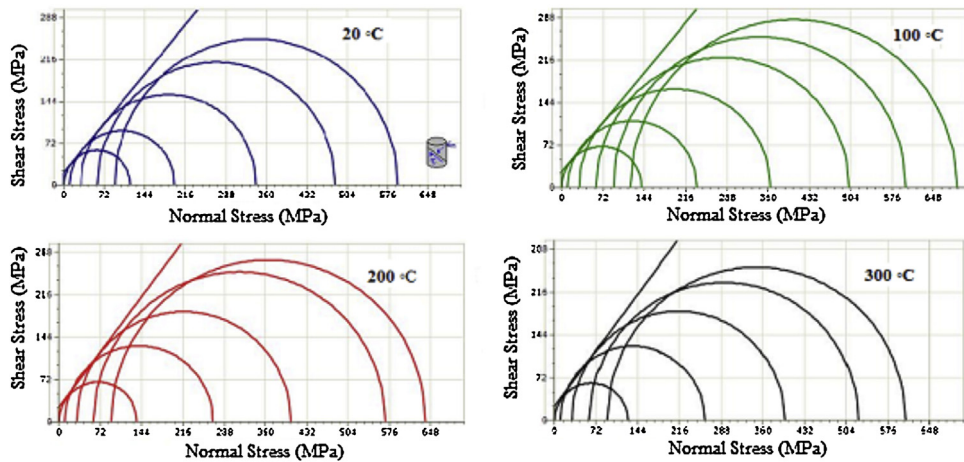


Fig. 9. Corresponding Mohr–Coulomb failure envelopes.

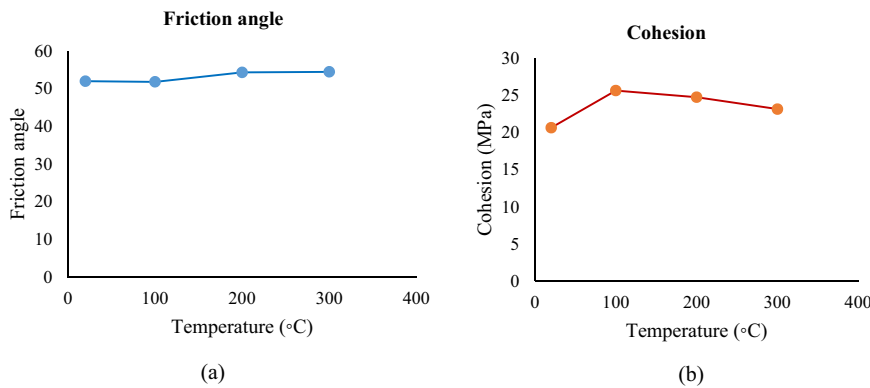


Fig. 10. Variation in (a) friction angle and (b) cohesion with different temperatures (considering linear region of the Mohr Coulomb failure envelope).

ments non-linearity must be taken into account. In addition to the confinement, according to this study, increasing temperature also alters the failure envelope of granite. An initial increment in deviatoric stress with increasing temperature can be observed up to 200 °C and further increase of temperature (to 300 °C) causes it to be slightly reduced.

The temperature-dependent shear parameters of granite were investigated next, and the shear parameters can be obtained from the Mohr-Coulomb failure envelope. As suggested by Singh et al. (2011), the Mohr-Coulomb parameters (cohesion and friction angle) were calculated using Eq. (1), taking into account the linear region of the obtained Mohr-Coulomb failure envelope (considering only smaller confining stresses, up to 30 MPa) for each temperature condition to obtain the temperature-dependent shear strength parameters (Fig. 10).

$$\sigma_1 = \frac{2C\cos\phi}{1-\sin\phi_i} + \frac{1+\sin\phi}{1-\sin\phi}\sigma_3 \quad (1)$$

where, σ_1, σ_3 are major principal stress and minor principal stress, and C and ϕ are cohesion and friction angle, respectively.

According to Fig. 10, cohesion increases from 20.7 to 25.7 MPa with increasing temperature from room temperature to 100 °C and further increases of temperature up to 200 °C and 300 °C cause the granite cohesion to be reduced to 24.8 MPa and 23.2 MPa, respectively. The observed cohesion gain at relatively low temperatures confirms that thermally-induced rock matrix expansion induces a greater mutual attraction among individual minerals. This is also influenced by the inhibition of micro-crack propagation at relatively low temperatures (Duclos and Paquet, 1991). In relation to

the latter positive effect of temperature on cohesion, according to Wong and Brace (1979), increasing the temperature to an extreme value may cause weakening of the grain boundaries, dependent on the anisotropy of the rock matrix (due to potentially existing distinct mineral compounds in granite those may contain different thermo-elastic moduli and this may causes to generate different internal stresses with heating). According to Wong and Brace (1979), increasing the temperature causes the induction of thermal cracks in the rock mass due to the associated generation of internal stresses (Eq. (2)):

$$\sigma = E\Delta\alpha\Delta T \quad (2)$$

where, E , $\Delta\alpha$, ΔT is the matrix Young's modulus, difference of thermal expansion coefficient of distinct mineral and temperature difference, respectively. When the internal stress (given by Eq. (2)) exceeds the crack closure pressure with increasing temperature, thermal cracks form and further increase of temperature provides the surface energy required for the propagation of the initiated crack (Zuo et al., 2007). This results in alteration of the grain-to-grain contacts in the rock matrix, which leads to reduced cohesion at higher temperatures. In the case of the variation of friction angle with increasing temperature, the granite friction angle appears to remain steady up to around 100 °C (52°) and then slightly increases with increasing temperature (54° at 200 and 300 °C, respectively). The friction between grain-to-grain contacts may be altered by the thermally-induced micro-structural modifications. However, this effect on grain contact is expected to be smaller at relatively low temperatures, resulting in relatively steady friction angle with increasing temperature at lower temperatures. However, a slight

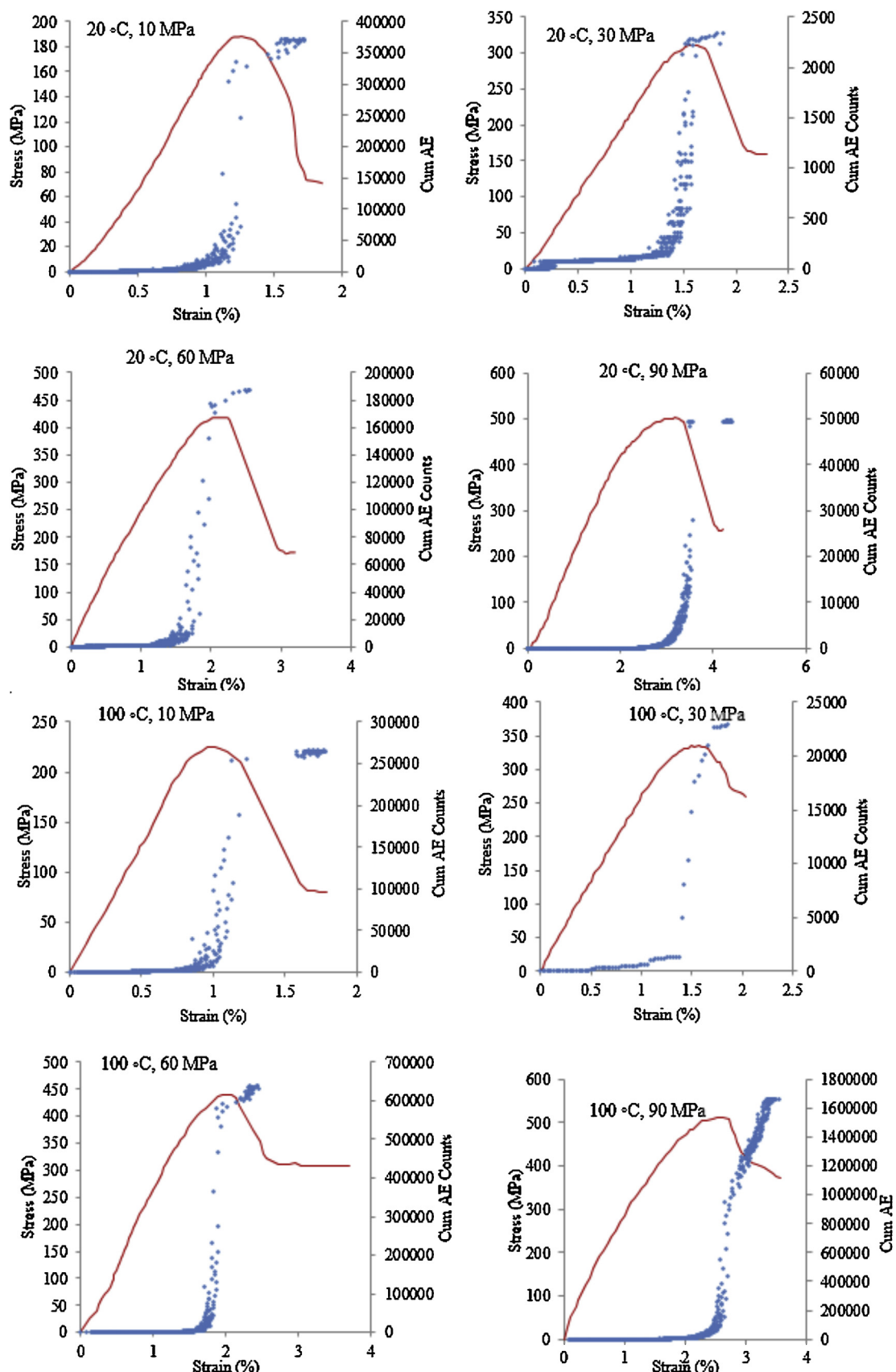


Fig. 11. Cumulative AE events vs. axial stress at different pressures and temperatures.

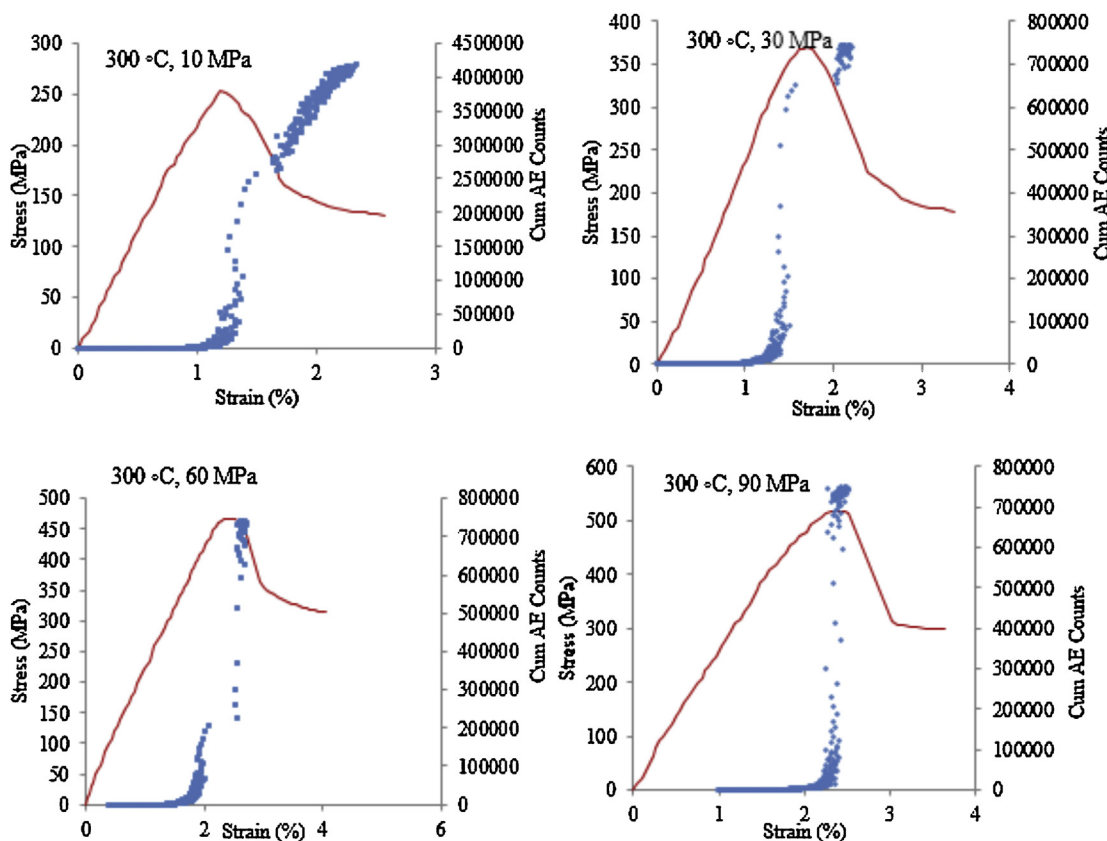


Fig. 11. (Continued)

enhancement in friction angle with increasing temperature can be seen, probably due to the increased resistance of mineral particles to external deformation as a result of the thermally-induced energy in the mineral particles. However, compared with cohesion, the temperature dependency on friction angle is relatively insignificant within the temperature region considered here.

Initial enhancement in shear parameters in sandstone with increasing temperature has been observed by [Zhang et al. \(2015\)](#) at relatively low temperature regions, and these researchers observed a reduction in friction angle from 33.02° to 31.93° and an increment in cohesion from 61.47 MPa to 66.44 MPa with increasing temperature from 25°C to 100°C . Further, [Bauer and Johnson \(1979\)](#) observed around 10% reduction in cohesion and 40% reduction in friction angle in Westerly granite with increasing temperature from room temperature to 300°C , and [Friedman et al. \(1979\)](#) observed a 7% reduction in cohesion and a 38% reduction in friction angle with increasing temperature from room temperature to 400°C and 300°C , respectively. However, the variation of shear strength parameters with increasing temperature at relatively low temperatures ($<300^\circ\text{C}$) was not considered in the above studies. The observed initial shear strengthening may be due to the inhibition of micro-crack propagation by the plasticity mechanism which occurs at crack tips ([Duclos and Paquet \(1991\)](#)) at low temperatures. With further increment of temperature, the reduction of shear strength parameters can be expected, due to the thermal weakening of the rock micro-structure. Furthermore, according to the SEM studies conducted by [Zuo et al. \(2007\)](#), large local plastic deformations and extremely rough cleavage fractures occur at relatively low temperatures. Moreover, due to the volume expansion, the distance between the interfaces of the individual minerals decreases with the enhancement of their mutual attraction, and the strength of the bonds increases ([Dmitriev, 1972](#)). Both of these phenomena can

be considered to explain the stress strengthening of granite under relatively low temperatures when subjected to confining pressures.

3.4. Analysis of fracturing behaviour using AE technology

Acoustic emission (AE) detection technology is a powerful non-destructive tool to study crack propagation processes in brittle materials, including the stages of crack initiation, growth and crack damage ([Lockner, 1993](#)). When a brittle material is under stress, strain energy is released during the development of new cracks or the widening of existing cracks. This energy is released in the form of elastic stress waves from the crack tips, and can be captured and amplified by an AE system. AE detection technology has therefore been widely used in a number of previous studies to understand the crack development mechanism in brittle materials ([Chang and Lee, 2004](#); [Lei et al., 2000](#); [Moura et al., 2005](#)).

By incorporating the crack propagation pattern into the stress-strain relationship of the cracking material, the crack development process can be divided into several stages. [Hoek and Bieniawski \(1965\)](#) divided crack formation into five main stages: crack closure, crack initiation, secondary cracking, crack coalescence and crack damage. Later, [Ranjith et al. \(2008\)](#) and [Shao et al. \(2015\)](#) incorporated stress-strain curves into cumulative AE counts/energy and strain plots. In the crack propagation process, with the gradual increment of loading on brittle materials, most pre-existing cracks are first closed, releasing an insignificant number of AE counts. This initial crack closure period is followed by the stable crack propagation period, which can be identified by the release of gradual AE energy increments. Further increment of loading causes an exponential increase in AE energy, indicating an unstable crack propagation period with failure approaching. The crack closure threshold (σ_{cc}) is defined as the stress threshold at which the initial AE counts are identified. An initial increment in cumulative AE

counts can be seen at the crack initiation (σ_{ci}) threshold, and the cumulative AE counts starts exponential growth at the crack damage (σ_{cd}) threshold. The region between the crack closure threshold and the crack initiation threshold is generally defined as the stable crack closure region, where linear elastic deformation occurs. The region between the crack initiation threshold and the crack damage threshold is defined as the stable crack propagation region, and the region between the crack damage threshold and sample failure is identified as the unstable crack propagation region.

The application of compressive loading fails rocks through either shear localization (brittle regime) or cataclastic flow, and the surrounding conditions, such as temperatures and pressures, may cause a homogenous plastic flow. According to existing studies, axial intra-granular cracking and shear rupturing of cemented grain contacts can be observed before failure in brittle regimes, and grain crushing and pore collapse can be identified before failure in cataclastic flow regimes (Menéndez et al., 1996). According to Wong et al. (1997), the development of local stress concentrations leads to the initiation of many intra-granular micro-cracks in the rock mass, and the crack density increases with increasing deviatoric stress and tends to merge on reaching the peak stress, resulting in strain softening and shear localization. These damage processes are clearly identified by the intense AE activities in the field (Chang and Lee, 2004). AE technology was therefore used to investigate the progressive fracturing behaviour in Strathbogie granite under tri-axial conditions. Fig. 11 illustrates the cumulative AE events with axial stress at various pressures and temperatures for the tested specimens. The corresponding variations of deviatoric stress against strain are also included in the same plots to identify the stress thresholds for crack closure, crack initiation and crack damage (Table 4). The very high AE counts in Strathbogie granite at dilatancy in the pre-failure stage are due to the fact that AE waves generate when the local shear stress concentration at a grain contact is sufficiently high to rupture the grain boundaries, and frictional slips and grain rotations may occur once the grain contacts have lost their cohesion.

In the present study, crack threshold ratios were defined to identify the temperature and pressure-dependent crack propagation in the tested granite as follows, and Fig. 12 shows the crack propagation stress threshold ratios of granite specimens tested at various confining pressures and temperatures.

$$\text{Crack closure stress threshold} = \frac{\text{Deviatoric stress at crack closure stress } (\sigma_{cc})}{\text{Deviatoric stress at failure}}$$

$$\text{Crack initiation stress threshold} = \frac{\text{Deviatoric stress at crack initiation stress } (\sigma_{ci})}{\text{Deviatoric stress at failure}}$$

$$\text{Crack damage stress threshold} = \frac{\text{Deviatoric stress at crack damage stress } (\sigma_{cd})}{\text{Deviatoric stress at failure}}$$

According to the results, the beginning of crack damage occurs at earlier stages of deviatoric loading for higher confining pressures. However, the crack damage stress increases with increasing confinement due to the influence of confining pressure on thermal crack development and the suppression of the extension/widening of existing micro-cracks. According to Fig. 12, in the temperature range considered here, three tendencies can be identified with increasing confining pressure: increase of the elastic deformation region, decrease of the stable crack propagation region, and increase of the unstable crack propagation region. The crack initiation stress threshold also progressively increases with increasing confining pressure, which can be attributed to the fact that the brittle behaviour of rock specimens at lower confining pressures changes to quasi-brittle behaviour with increasing confining pressure. This is because the suppression of micro-crack development is less at low confining pressures, and therefore sudden failures mostly occur, and the beginning of crack initiation occurs

at earlier stages of deviatoric loading at high confining pressures due to the higher normal stress acting on micro-cracks, resulting in limited progression of cracking before failure. In relation to the temperature effect, increasing the temperature causes an initial increment in the crack propagation stress threshold, followed by a slight reduction for all the temperature conditions considered. For example, at 30 MPa confinement, the crack damage stress threshold ratios increased by around 6.8%, 10.5% with increasing temperature from room temperature to 100 and 200 °C, respectively, and reduced by around 4.0% when the temperature increased to 300 °C. This implies that at low temperatures a suppressed micro-crack development mechanism is dominant, and increasing the temperature causes crack damage to occur at earlier loading stages. Interestingly, at 60 MPa confinement the crack damage stress threshold ratio increased by around 4.9%, 5.4%, 2.6% with increasing temperature from room to 100, 200 and 300 °C, respectively. This exhibits the cumulative effect of temperature and pressure micro-crack development in the rock mass. At relatively low temperatures, micro-crack propagation may be inhibited by the thermally-induced plasticity mechanism which occurs at crack tips and the increased bonding strength through thermally-induced rock matrix expansion (which increases crack stress thresholds). However, further increase of temperature creates thermally-induced cracks and causes the grain boundary cracks to widen, resulting in early crack damage. Further, with the influence of confinement, micro-crack development is suppressed, causing a relatively low increment of crack damage stress threshold ratios at higher confinements.

3.5. Corresponding alterations in granite micro-structure

A comprehensive micro-structural analysis was also performed to identify the interior correspondences of the above-described temperature-dependent mechanical behaviour of granite. SEM and optical microscopic analyses were performed on thin sections of granite specimens at various temperatures: room temperature (20 °C), pre-heated (72 hours) to 200 °C and 400 °C (Fig. 13). These temperatures were selected to identify the microstructural behaviour at 200 °C, at which the highest strength increment was observed, and 400 °C, at which clear thermally-induced rock mass weakening was observed. A specimen at room temperature was used as a control.

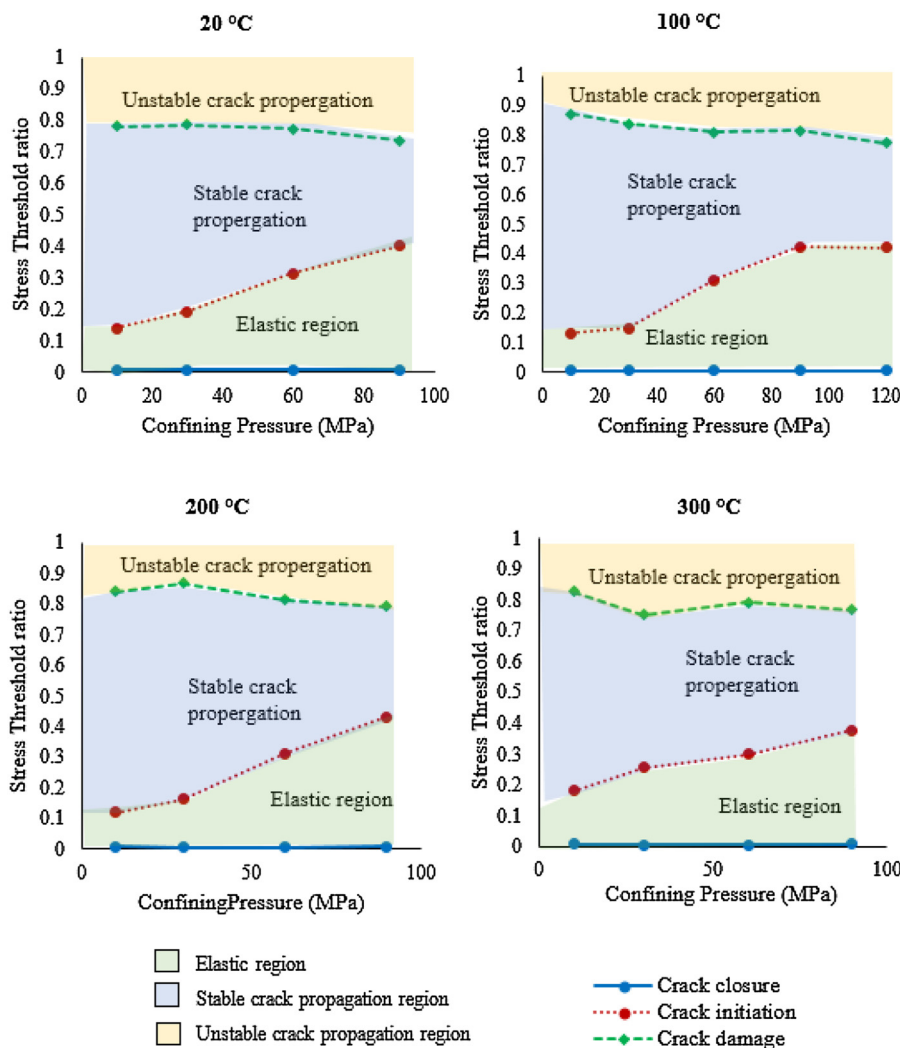
Based on optical microscope imaging, mineralogical assembling in the granite specimen could be identified by the colour and texture of each of the mineral assemblages. Further, a detailed SEM study was performed using scanning electron imaging (SEI) and BSEI back-scatter electron imaging (BSEI) techniques. BSEI images taken at low magnifications clearly show different mineral assemblages and grain boundaries (see Fig. 14). Using energy-dispersive X-ray (EDX) technology with Aztec Oxford instruments, chemical component mapping was generated in each specimen, and each mineral was identified qualitatively. The bright colour images observed in EDX images indicate higher concentration (higher energy dispersion) while dark colour areas indicate lower concentration (lower energy dispersion). Based on the spectrum of each point (point ID), the corresponding mineral was identified and a map spectrum provided overall elements available for each specimen.

According to Figs. 13 and 14, there are clear mineralogical assembling in the granite specimens, mainly with quartz, K-feldspar and plagioclase. The heating of granite up to 200 °C temperature has not caused any significant thermally-induced micro-cracks (in addition to the pre-existing faults and grain boundaries) and almost all grain boundaries remain intact. However, further heating of granite to the higher temperature of 400 °C caused the induction of some micro-cracks, mainly along

Table 4

Stress thresholds for different fracturing stages.

Temperature (°C)	Confining Pressure (MPa)	Deviatoric stress at failure (MPa)	Crack closure threshold (σ_{cc}) (MPa)	Crack initiation threshold (σ_{ci}) (MPa)	Crack damage threshold (σ_{cd}) (MPa)
20	10	186.9	1.3	25.9	146.0
	30	311.9	1.8	59.4	244.5
	60	422.5	2.6	131.7	325.7
	90	503.3	3.8	202.0	370.0
100	10	225.5	1.4	29.8	196.0
	30	333.7	1.9	50.3	279.4
	60	440.9	2.6	137.2	356.5
	90	510.3	3.9	216.0	415.1
	120	568.9	4.0	239.2	439.0
200	10	258.2	1.6	30.8	217.4
	30	374.4	1.9	61.2	324.5
	60	509.0	2.8	158.0	413.6
	90	549.6	3.6	237.1	434.4
300	10	249.4	0.03	45.2	206.3
	30	367.5	1.8	93.5	276.6
	60	464.6	2.4	139.1	367.7
	90	516.5	3.9	194.0	396.2

**Fig. 12.** Crack propagation stress threshold ratios of granite specimens tested at various confining pressures and temperatures.

the quartz and feldspar minerals (intra-granular cracks) and the quartz-feldspar grain boundaries (inter-granular cracks). Some grain boundary cracks running along grain boundaries and around

pore boundaries could be identified. A considerable number of cracks were propagated after 400 °C at triple junctions dominantly in quartz- feldspar boundaries. However, only a few grain

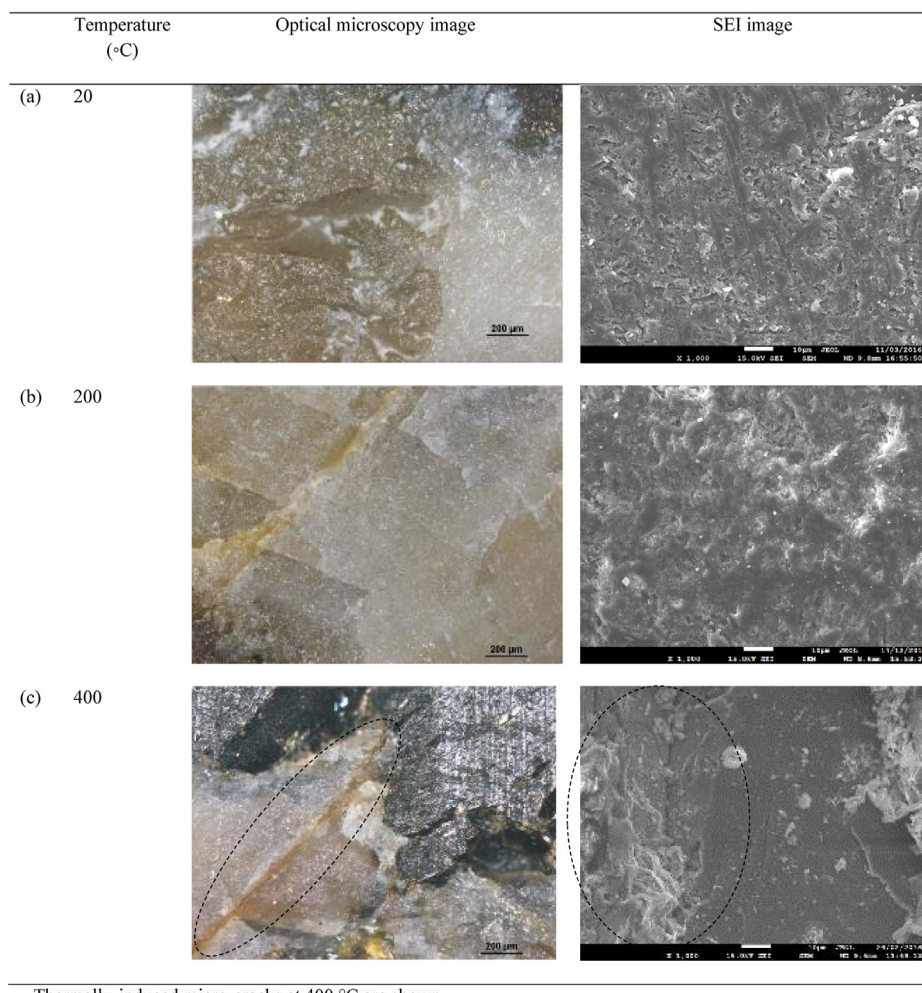


Fig. 13. Optical microscopic and SEM images of thin sections of Strathbogie granite (a) at room temperature; (b) pre-heated to 100 °C (c) pre-heated to 400 °C.

boundaries have been partially parted and a significant number of grain boundaries appear to remain intact up to this temperature. Furthermore, based on the EDX mapping, it was confirmed that intra-granular cracks are mainly initiated along the feldspar and quartz minerals. Intragranular cracks were mainly observed in larger crystals (crystals greater than 0.5 mm) and smaller crystals remained un-parted even at 400 °C. For Strathbogie granite, thermally-induced intra-granular micro-cracks seem to play a significant role at relatively low temperatures, probably due to the presence of relatively high K feldspar and biotite contents. Similar observations have been reported in Bauer and Johnson's (1979) study conducted for Charcoal granite, where intra-granular micro-cracks predominantly occur compared to grain boundary cracks. The SEM analysis is also consistent with this finding, which exhibits inhibition of micro-crack development followed by micro-cracking at relatively high temperatures.

The crack propagation process in any rock mass is largely influenced by the mineralogical composition, because cracks normally propagate through weaker planes of the rock mass. Since granite is an igneous type of rock, two main types of thermally-induced cracking modes can be identified: inter-granular and intra-granular. The amount of inter-granular or intra-granular cracking is dependent on the stress state, rock type and mineralogy of the rock mass. Inter-granular cracks occur along grain boundaries, pre-existing faults and micro-cracks of the rock, while intra-granular cracks occur through weaker mineralogical constituents (Kranz, 1983). For example, K- feldspar and biotite are weaker

mineralogical constituents due to their large crystals (>10 mm), as crystals greater than 2–3 mm in size are generally defined as weaker mineralogical constituents compared to equi-dimensional small crystals like quartz (Homand-Etienne and Houpert, 1989). Based on experimental results, intra-granular cracking is highly temperature-dependent due to the temperature-dependent dislocations in the rocks. This is because different mineralogical components have different thermo-elastic moduli and thermal conductivities (Kranz, 1983; Dwivedi et al., 2008).

These observations suggest that micro-cracking in granite is highly temperature-dependent, as evidenced by the previously observed initial strength gain followed by slight strength reduction with increasing temperature in the tested granite. However, this shows that granite needs to be heated to a sufficient temperature to cause thermal cracks in it and therefore, heating to a lower temperature may only cause a strength gain through the thermal expansion of the rock matrix. This is consistent with the results of Bauer and Johnson (1979). The mechanical properties of Charcoal granite in their study remained relatively steady until 200 °C, and Westerly granite exhibited a significant thermal dependency, even at relatively low temperatures (<200 °C). In Homand-Etienne and Houpert (1989) study, the variation of uni-axial compressive strength of both Semones and Remiremont granites is insignificant until 400 °C, followed by significant reductions at higher temperatures. These results indicate the dependency of mineralogical composition and grain size distribution on the temperature-dependent mechanical behaviour in various types of granites. However,

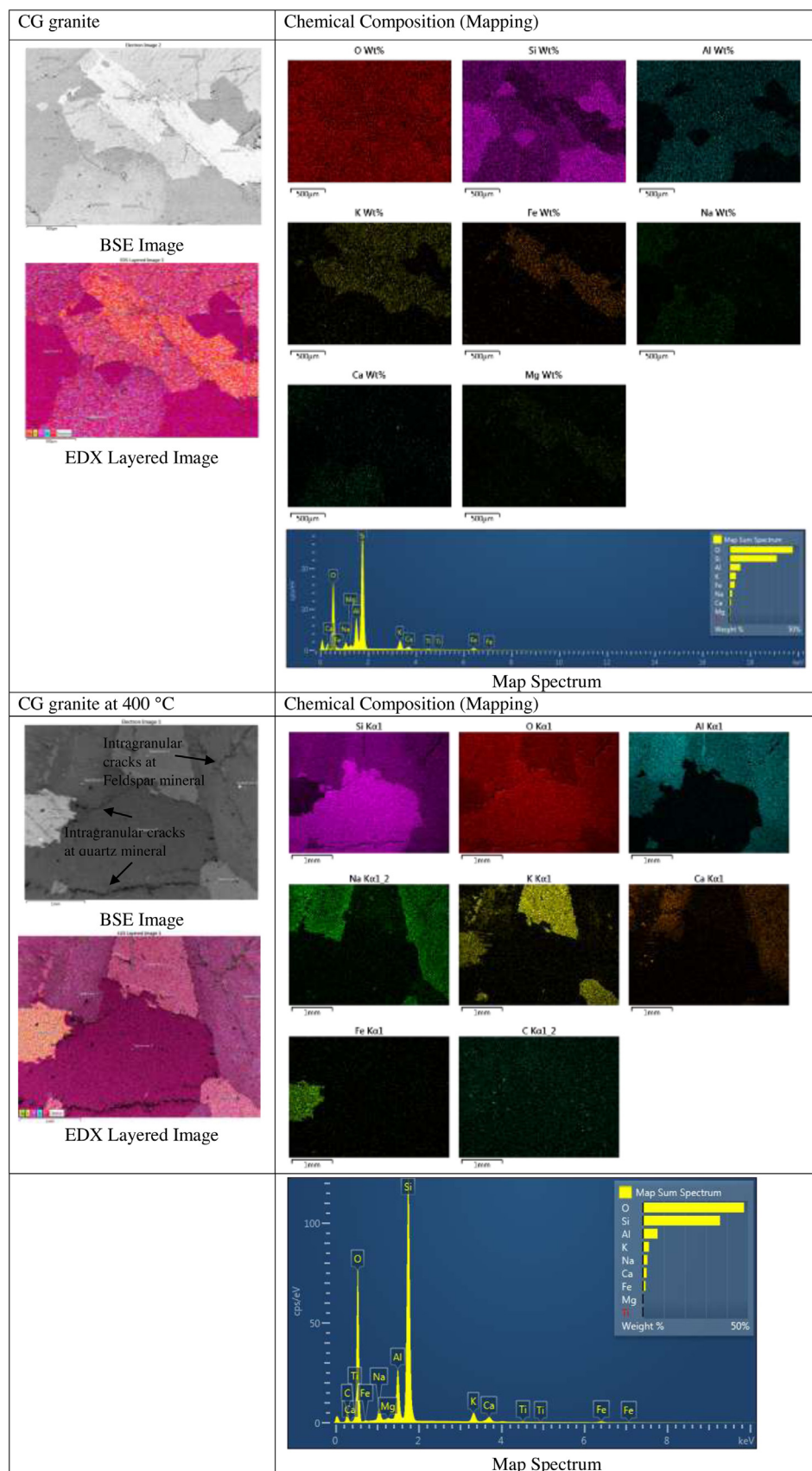


Fig. 14. BSE images of Strathbogie granite with EDX mapping: (a) thin section at room temperature; (c) thin section pre-heated to 400 °C.

all the existing studies described above were conducted on pre-heated specimens, which really cannot represent the real in-situ field situation in geothermal reservoirs. The present study may therefore capture more realistic geothermal reservoir behaviour.

3.6. Temperature-dependent failure criteria for Strathbogie granite

To date, although many strength criteria are available for intact rock, the practical application of most of them for geothermal reservoirs is questionable, due to the in-situ model parameters required when considering the available high-pressure and high-temperature environment in underground reservoirs. Of the various failure criteria, the Mohr-Coulomb failure criteria have been extensively used in the field and have made a significant contribution to the determination of rock mass failure. However, they have some major limitations, including ignoring the intermediate stress σ_2 influence (which has been proven to have a substantial influence on rock strength) and the assumed linearity (the strength criteria of rock are non-linear in reality). After re-analyzing thousands of reported triaxial experiments and combining the critical state concept proposed by Barton (1976), Singh et al. (2011) proposed a non-linear Mohr-Coulomb failure criterion. According to the findings of Singh et al. (2011), the Mohr-Coulomb shear strength parameters should only be obtained by performing conventional tri-axial tests under low confining stresses (in the linear region of the Mohr-Coulomb failure envelope). According to their statistical analysis, $\sigma_{cc} \approx \sigma_{crit}$, where σ_c and σ_{crit} are uni-axial compressive strength and critical confining pressure, respectively. The modified Mohr-Coulomb failure criterion proposed by Singh et al. is given below:

$$\sigma_1 - \sigma_3 = \sigma_{ci} + \frac{2\sin\phi_{i0}}{1 - \sin\phi_{i0}} \sigma_3 - \frac{2\sin\phi_{i0}}{\sigma_{crit}(1 - \sin\phi_{i0})} \sigma_3^2 \quad \text{for } 0 \leq \sigma_3 \leq \sigma_{crit} \quad (3)$$

where, $\sigma_{ci} \approx \text{UCS}$ of the rock = $2C_{io}\cos\phi_{i0}/1 - \sin\phi_{i0}$, ϕ_{i0} and C_{io} are friction angle and cohesion obtained at low confining pressures.

However, even the improved Mohr-Coulomb failure criteria cannot be directly applied to geothermal reservoir rocks at extreme pressures and temperatures, because the strength response is altered by the thermal effect (Heuze, 1983). To date, no extensive study has captured this thermal response in the improved Mohr-Coulomb failure criteria. Such a realistic approach is necessary for deep underground engineering applications like geothermal energy extraction. The concepts of Barton (1976) and Singh et al. (2011) are therefore incorporated into the temperature influence in this study and an attempt is made to propose novel strength criteria for geothermal reservoir rocks based on experimental data:

$$\sigma_1 - \sigma_3(T) = \frac{2C_i(T)\cos\phi_i(T)}{1 - \sin\phi_i(T)} + \frac{2\sin\phi_i(T)}{1 - \sin\phi_i(T)} \sigma_3 - \frac{2\sin\phi_i(T)}{\sigma_{crit}(T)(1 - \sin\phi_i(T))} \sigma_3^2 \quad \text{for } 0 \leq \sigma_3 \leq \sigma_{crit} \quad (4)$$

where, $\phi_i(T)$, $C_i(T)$ and $\sigma_{crit}(T)$ are temperature-dependent friction angle, cohesion and critical confining pressure and can be given as follows:

$$\frac{\phi_i(T)}{\phi_{i0}} = f_1(T) = 1.034 - 0.0032T + 3.53 \times 10^{-5}T^2 - 7.62 \times 10^{-8}T^3 \quad (5)$$

$$\frac{C_i(T)}{C_{io}} = f_2(T) = 0.7795 + 0.1504T - 0.0001T^2 + 2.22 \times 10^{-8}T^3 \quad (6)$$

$$\frac{\sigma_{crit}(T)}{\text{UCS}} = f_3(T) = 1.7887 + 0.0226T - 0.0002T^2 + 4.52 \times 10^{-7}T^3 \quad (7)$$

However, it should be noticed that the modified temperature-dependent criteria may only be applicable for similar types of granites under the tested experimental conditions.

4. Conclusions

A series of tri-axial strength tests was conducted on Australian Strathbogie granite under four different confining pressures (10, 30, 60, 90 MPa) and four different temperatures (RT, 100, 200, 300 °C), simulating various geothermal reservoir conditions. The following conclusions can be drawn:

- Mechanical behaviour of the tested granite is influenced by both reservoir depth and temperature, and the depth effect is much greater than the temperature effect.
- Granite located at relatively smaller depths appears to fail through shear localization and increasing depth may cause this to change to ductile failure through strain hardening. A progressive enhancement in stress threshold with increasing confining pressure is observed in Strathbogie granite. Such behaviours exhibit greater strength and lower brittle characteristics in granite located at greater depths.
- Increasing of temperature causes granite's strength to be enhanced up to a certain temperature (around 200 °C for Strathbogie granite) through the possible thermal expansion of the rock matrix and further increasing of temperature may cause it to weaken by inducing thermal cracks. This was confirmed by the micro-structural analysis, which did not reveal any noticeable amount of thermally-induced micro-cracking in Strathbogie granite up to 200 °C, and heating of the granite to a greater temperature as 400 °C caused many intra-granular cracks in quartz and feldspar and some grain boundary cracks between quartz and feldspar minerals. Furthermore, according to AE analysis, increasing the temperature first causes the crack propagation stress threshold to increase and further increasing of the temperature causes it to be slightly reduced. This indicates a suppression of micro-cracks at low temperatures by matrix expansion and the development of micro-cracks through thermally-induced damage at higher temperatures.
- Finally an attempt was made to improve the conventional Mohr-Coulomb failure criteria for geothermal reservoirs with extreme pressures and temperatures, because the conventional criteria are not applicable to extreme conditions.

Acknowledgements

This research project is funded by the Australian Research Council (ARC- DP160104223) and the authors would like to thank all the Deep Earth Energy Laboratory staff at Monash University, Clayton campus, Australia and the Monash Centre for Electron Microscopy (MCEM), who dedicated their time and energy to bring this experimental series to a successful conclusion. The sixth author extends his appreciation to the Deanship of Scientific Research at King Saud University (Saudi Arabia) for funding the work through the international research group project no. IRG14-36.

References

- ASTM D7012-10, 2010. Standard test method for compressive strength and elastic moduli of intact rock core specimens under varying states of stress and temperatures. In: Annual Book of ASTM Standards. American Society for Testing and Materials, West Conshohocken, PA.
- Axelsson, G., 2010. Sustainable geothermal utilization—case histories; definitions; research issues and modelling. Geothermics 39, 283–291.
- Barton, N., 1976. The shear strength of rock and rock joints. Int. J. Rock Mech. Min. Sci. Geomech. Abstr. 13, 255–279.
- Barton, N., 2013. Shear strength criteria for rock, rock joints, rockfill and rock masses: problems and some solutions. J. Rock Mech. Geotech. Eng. 5, 249–261.
- Bauer, S., Johnson, B., 1979. Effects of slow uniform heating on the physical properties of the Westerly and Charcoal granites, 20th US Symposium on Rock Mechanics (USRMS). Am. Rock Mech. Assoc., 7–18.
- Best, M.G., 1995. Igneous and Metamorphic Petrology. Blackwell Science Cambridge, MA.

- Breede, K., Dzebisashvili, K., Liu, X., Falcone, G., 2013. A systematic review of enhanced (or engineered) geothermal systems: past, present and future. *Geotherm. Energy* 1, 1–27.
- Chang, S.-H., Lee, C.-I., 2004. Estimation of cracking and damage mechanisms in rock under triaxial compression by moment tensor analysis of acoustic emission. *Int. J. Rock Mech. Min. Sci.* 41, 1069–1086.
- Chester, F., Higgs, N., 1992. Multimechanism friction constitutive model for ultrafine quartz gouge at hypocentral conditions. *J. Geophys. Res.: Solid Earth* (1978–2012) 97, 1859–1870.
- Dai, Z., Stauffer, P.H., Carey, J.W., Middleton, R.S., Lu, Z., Jacobs, J.F., Hnottavange-Telleen, K., Spangle, L., 2014. Pre-site characterization risk analysis for commercial-scale carbon sequestration. *Environ. Sci. Technol.* 48, 3908–3915.
- Dmitriev, A.P., 1972. *Physical Properties of Rocks at High Temperatures*. National Aeronautics and Space Administration; National Technical Information Service, Springfield, VA.
- Duclos, R., Paquet, J., 1991. High-temperature behaviour of basalts—role of temperature and strain rate on compressive strength and K IC toughness of partially glassy basalts at atmospheric pressure. *Int. J. Rock Mech. Min. Sci. Geomech. Abstr.* 28, 71–76.
- Dwivedi, R.D., Goel, R.K., Prasad, V.V.R., Sinha, A., 2008. Thermo-mechanical properties of Indian and other granites. *Int. J. Rock Mech. Min. Sci.* 45, 303–315.
- Fox, D.B., Sutter, D., Beckers, K.F., Lukawski, M.Z., Koch, D.L., Anderson, B.J., Tester, J.W., 2013. Sustainable heat farming: modeling extraction and recovery in discretely fractured geothermal reservoirs. *Geothermics* 46, 42–54.
- Friedman, M., Handin, J., Higgs, N., Lantz, J., 1979. Strength and ductility of four dry igneous rocks at low pressures and temperatures to partial melting, 20th US Symposium on Rock Mechanics (USRMS). Am. Rock Mech. Assoc., 35–43.
- Gajo, A., Bigoni, D., Wood, D.M., 2004. Multiple shear band and related instabilities in granular materials. *J. Mech. Phys. Solids* 52, 2683–2724.
- Heard, H., Page, L., 1982. Elastic moduli, thermal expansion, and inferred permeability of two granites to 350 °C and 55 megapascals. *J. Geophys. Res.: Solid Earth* (1978–2012) 87, 9340–9348.
- Heuze, F., 1983. High-temperature mechanical, physical and thermal properties of granitic rocks—a review. *Int. J. Rock Mech. Min. Sci. Geomech. Abstr.* 20, 3–10, Elsevier.
- Hoek, E., Bierniawski, Z., 1965. Brittle fracture propagation in rock under compression. *Int. J. Fract. Mech.* 1, 137–155.
- Hoek, E., 1983. Strength of jointed rock masses. *Geotechnique* 33, 187–223.
- Homand-Etienne, F., Houpert, R., 1989. Thermally induced microcracking in granites: characterization and analysis. *Int. J. Rock Mech. Min. Sci. Geomech. Abstr.* 26, 125–134.
- Klein, E., Baud, P., Reuschlé, T., Wong, T.F., 2001. Mechanical behaviour and failure mode of bentheim sandstone under triaxial compression. *Phys. Chem. Earth Part A* 26, 21–25.
- Kranz, R.L., 1983. Microcracks in rocks: a review. *Tectonophysics* 100, 449–480.
- Lei, X.L., Kusunose, K., Nishizawa, O., Cho, A., Satoh, T., 2000. On the spatio-temporal distribution of acoustic emissions in two granitic rocks under triaxial compression: the role of pre-existing cracks. *Geophys. Res. Lett.* 27, 1997–2000.
- Lockner, D., 1993. The role of acoustic emission in the study of rock fracture. *Int. J. Rock Mech. Min. Sci. Geomech. Abstr.* 30, 883–899.
- Martín-Gamboa, M., Iribarren, D., Dufour, J., 2015. On the environmental suitability of high-and low-enthalpy geothermal systems. *Geothermics* 53, 27–37.
- Menéndez, B., Zhu, W., Wong, T.-F., 1996. Micromechanics of brittle faulting and cataclastic flow in Berea sandstone. *J. Struct. Geol.* 18, 1–16.
- Mogi, K., 1966. Pressure dependence of rock strength and transition from brittle fracture to ductile flow. *Bull. Earthq. Res. Inst. Tokyo* 44 (1966), 215–232.
- Moura, A., Lei, X., Nishisawa, O., 2005. Prediction scheme for the catastrophic failure of highly loaded brittle materials or rocks. *J. Mech. Phys. Solids* 53, 2435–2455.
- Paquet, J., François, P., 1980. Experimental deformation of partially melted granitic rocks at 600–900 °C and 250 MPa confining pressure. *Tectonophysics* 68, 131–146.
- Paterson, M.S., Wong, T.-F., 2005. *Experimental Rock Deformation: the Brittle Field*. Springer Science & Business Media, Berlin.
- Phillips, G.N., Wall, V.J., Clemens, J.D., 1981. Petrology of the Strathbogie batholith: a cordierite-bearing granite. *Can. Mineral.* 19, 51–79.
- Ranjith, P.G., Jasinge, D., Song, J.Y., Choi, S.K., 2008. A study of the effect of displacement rate and moisture content on the mechanical properties of concrete: use of acoustic emission. *Mech. Mater.* 40, 453–469.
- Shao, S., Wasantha, P.L.P., Ranjith, P.G., Chen, B.K., 2014. Effect of cooling rate on the mechanical behavior of heated Strathbogie granite with different grain sizes. *Int. J. Rock Mech. Min. Sci.* 70, 381–387.
- Shao, S., Ranjith, P.G., Wasantha, P.L.P., Chen, B.K., 2015. Experimental and numerical studies on the mechanical behaviour of Australian Strathbogie granite at high temperatures: an application to geothermal energy. *Geothermics* 54, 96–108.
- Singh, M., Raj, A., Singh, B., 2011. Modified Mohr–Coulomb criterion for non-linear triaxial and polyaxial strength of intact rocks. *Int. J. Rock Mech. Min. Sci.* 48, 546–555.
- Singh, B., Ranjith, P., Chandrasekharan, D., Viete, D., Singh, H., Lashin, A., Al Arifi, N., 2015. Thermo-mechanical properties of Bundelkhand granite near Jhansi, India. *Geomech. Geophys. Geo-Energy Geo-Resour.* 1, 35–53.
- Siratovich, P., Heap, M., Villeneuve, M., Cole, J., Kennedy, B., Davidson, J., Reuschlé, T., 2016. Mechanical behaviour of the Rotokawa Andesites (New Zealand): insight into permeability evolution and stress-induced behaviour in an actively utilised geothermal reservoir. *Geothermics* 64, 163–179.
- Tian, H., Kempka, T., Xu, N., Ziegler, M., 2013. *A Modified Mohr–Coulomb Failure Criterion for Intact Granites Exposed to High Temperatures*. Springer Series in Geomechanics and Geoengineering, Berlin, pp. 379–393.
- Tullis, J., Yund, R.A., 1977. Experimental deformation of dry Westerly granite. *J. Geophys. Res.* 82, 5705–5718.
- Vásárhelyi, B., Kovács, L., Török, A., 2016. Analysing the modified Hoek–Brown failure criteria using Hungarian granitic rocks. *Geomech. Geophys. Geo-Energy Geo-Resour.* 2, 1–6.
- Wawersik, W.R., Hannum, D.W., 1980. Mechanical behavior of New Mexico rock salt in triaxial compression up to 200 °C. *J. Geophys. Res.: Solid Earth* 85, 891–900.
- Wong, T.F., Brace, W., 1979. Thermal expansion of rocks: some measurements at high pressure. *Tectonophysics* 57, 95–117.
- Wong, T.F., David, C., Zhu, W., 1997. The transition from brittle faulting to cataclastic flow in porous sandstones: mechanical deformation. *J. Geophys. Res.: Solid Earth* (1978–2012) 102, 3009–3025.
- Wong, T.F., Baud, P., Klein, E., 2001. Localized failure modes in a compactant porous rock. *Geophys. Res. Lett.* 28, 2521–2524.
- Wong, T.F., 1982. Effects of temperature and pressure on failure and post-failure behavior of Westerly granite. *Mech. Mater.* 1, 3–17.
- Xu, X.L., Gao, F., Shen, X.-M., Xie, H.-P., 2008. Mechanical characteristics and microcosmic mechanisms of granite under temperature loads. *J. China Univ. Min. Technol.* 18, 413–417.
- Zhang, P., Mishra, B., Heasley, K.A., 2015. Experimental investigation on the influence of high pressure and high temperature on the mechanical properties of deep reservoir rocks. *Rock Mech. Rock Eng.* 48 (6), 2197–2211.
- Zuo, J., Xie, H., Zhou, H., Peng, S., 2007. Thermal-mechanical coupled effect on fracture mechanism and plastic characteristics of sandstone. *Sci. China Ser. E: Technol. Sci.* 50, 833–843.